Flux-Weakening in IPM Motor Drives: Comparison of State-of-Art Algorithms and a Novel Proposal for Controller Design

Silverio Bolognani[1], Roberto Petrella[2], Sandro Calligaro[2], Filippo Pogni[1]

[1]Dept. of Electrical Engineering, University of Padova, Italy
[2]Dept. of Eletrical, Management and Mechanical Engineering, University of Udine, Italy

Tel.: +39 049 8277509[1], +39 0432 558245[2]
Fax: +39 049 8277599[1], +39 0432 558251[2]
E-Mail: silverio.bolognani@unipd.it, roberto.petrella@uniud.it, sandro.calligaro@uniud.it, filippo.pogni@libero.it
URL: http://www.dieunipd.it[1], http://www.diegm.uniud.it[2]

Abstract

A review and comparison of some state-of-the-art flux-weakening algorithms for Interior Permanent Magnet Synchronous Motor (IPMSM) is presented in this paper, having voltage exploitation, dynamical performances and implementation efforts as key parameters of the comparison. Moreover an original proposal for the theoretical analysis of the overall dynamics of the voltage control loop is carried out, also taking into account non-linear effects and discrete-time implementation issues.
All the considered algorithms have at least one feed-back path, thus providing steady-state voltage control even in presence of parameter errors, but different strategies are adopted leading to completely different behavioral characteristics. The approaches that will be analyzed are based on the control of the synchronous reference frame currents, the torque-flux characteristics and the voltage space vector angle.
The effort for improving the voltage limitation performances, aiming at increasing dc bus voltage exploitation while still maintaining reasonable dynamical performances, is gaining importance due to both the efficiency demand (i.e. reducing the phase current magnitude for the required power) and some specific application issues, like the need for widening the speed-torque range given a relatively low voltage bus (e.g. in electrical or hybrid traction applications).
A motor drive system for home appliances is considered in this paper as test bench for comparing the reviewed techniques. Simulation and experimental results are included.

Keywords

« High speed drive», «Efficiency», «Electrical drive», «Synchronous motor»

Introduction

Interior permanent magnet (IPM) synchronous motors are often considered for those applications where wide constant-power speed range and high efficiency is required, such as in the vehicle traction applications or for home appliances (e.g. washing machines). Optimized machine control is obtained both below the base speed range (e.g. with maximum-torque-per-ampere (MTPA) control) and in flux-weakening range. In almost all the approaches a proper control of direct and quadrature components of the stator current space vector is considered.
The limited value of the reference voltage of the feeding inverter defines the constant apparent power region, i.e. the flux-weakening zone in which available motor torque decreases with the speed increase. Optimal design of the flux-weakening strategy aims at guaranteeing the maximum available voltage exploitation, thus providing the maximum torque for any given speed and minimizing the phase current magnitude (therefore reducing one of the main power losses).

Many algorithms for flux-weakening control of IPM motors have been proposed in literature, intended to satisfy this last requirement. The best performances are certainly provided by those methods adopting at least a feed-back approach [1]-[8] (but also incorporating feed-forward features, [3][4]) and often based on the direct control of the motor feeding voltage. Unfortunately, a comparative performance analysis of the most promising strategies as well as the study of the dynamical properties of the voltage regulation loop is today lacking, being the aim of this paper. Such a study is desirable in order to highlight the specific features of each method, also taking into account the implementation efforts, and to understand which is more suitable for a certain application. *A novel theoretical approach is also presented for the study and the optimization of the dynamical properties of the flux-weakening controller, thus allowing to maximize the inverter bus voltage exploitation whilst guaranteeing the stability of the system even in very high flux-weakening conditions*. Simulation by means of Matlab/Simulink tools and experimental results on a *dSpace* board controlled drive system are reported.

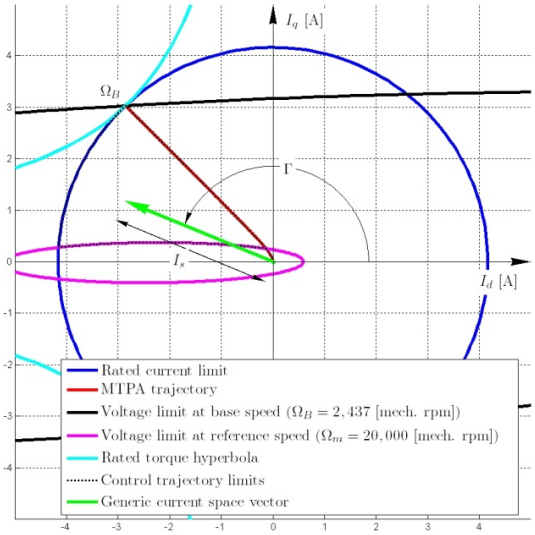

Fig. 1. Motor operating loci.

IPM synchronous motor model and operating limitations

The analytical model for an IPM motor in the synchronous dq reference frame can be represented by the following vector equation (the d axis is aligned with the rotor permanent magnet flux):

$$\bar{u}_{dq} = R\bar{\imath}_{dq} + \boldsymbol{L}\frac{d\bar{\imath}_{dq}}{dt} + \omega_{me}\boldsymbol{L}'\bar{\imath}_{dq} + \omega_{me}\bar{\lambda}_{mg} \tag{1}$$

where $\bar{u}_{dq}$, $\bar{\imath}_{dq}$ and $\bar{\lambda}_{mg}$ are voltage, current and permanent magnet flux linkage vectors, i.e.

$$\bar{u}_{dq} = \begin{bmatrix} u_d \\ u_q \end{bmatrix}, \bar{\imath}_{dq} = \begin{bmatrix} i_d \\ i_q \end{bmatrix}, \bar{\lambda}_{mg} = \begin{bmatrix} 0 \\ \Lambda_{mg} \end{bmatrix} \tag{2}$$

and matrices $\boldsymbol{L}$ and $\boldsymbol{L}' \triangleq \boldsymbol{JL}$ are related to motor synchronous inductances, i.e.:

$$\boldsymbol{L} = \begin{bmatrix} L_d & 0 \\ 0 & L_q \end{bmatrix}, \boldsymbol{J} = \begin{bmatrix} 0 & -1 \\ 1 & 0 \end{bmatrix}, \boldsymbol{JL} = \begin{bmatrix} 0 & -L_q \\ L_d & 0 \end{bmatrix} \tag{3}$$

Electromagnetic torque is therefore:

$$M_e = \frac{3}{2}pp\left[\Lambda_{mg}i_q + (L_d - L_q)i_d i_q\right] \tag{4}$$

where pp is the number of pole-pairs.

The maximum voltage U_N that the inverter can supply to the machine is limited by the DC link voltage (U_{dc}) and the adopted PWM strategy. When linear modulation is considered, so that the voltage vector always stays inside the inscribed circle in the limit hexagon, the maximum voltage value is $U_N = U_{dc}/\sqrt{3}$, while higher voltages can be obtained if a saturation (distortion) is allowed, moving towards the six-step modulation. The maximum current I_N is determined by the inverter current rating and the machine thermal rating.

Since the vector current control is usually implemented, the machine operating condition is normally studied by drawing the *current–limit locus* and *voltage–limit locus* in the I_d and I_q plane [5], as shown in Fig. 1. The former is represented by a circle with radius I_N and center in the origin, the latter by a set of ellipses whose size is inversely proportional to the electrical angular speed. The center of the ellipses is defined by the short circuit direct current $I_{cc} = -\Lambda_{mg}/L_d$.

In Fig. 1, the three different *current loci* can be identified, that set the operating region boundaries: the maximum-torque-per-ampere (MTPA) trajectory, the flux–weakening curve along the limit circle and the voltage limit ellipse at maximum speed. Along the first trajectory the available torque is constant (equal to the nominal torque M_N) up to a certain value of electrical motor speed (i.e. base speed, Ω_B) and amplitude of current and voltage space vectors is lower than machine limits. MTPA control

strategy is commonly adopted and the corresponding current operating points are on the red curve in Fig. 1. Above the base speed, maximum available torque is determined by the intersection of the current limit circle and the voltage limit ellipse. Depending on the torque command and operating speed, the working point can lie on the MTPA trajectory (for lower speed values) or in the space below it (i.e. having a higher phase angle), when field-weakening is needed. Therefore the maximum torque decreases with speed. The aim of the flux-weakening control is to provide correct operation with the maximum available torque at any speed (within current and voltage limits) by means of a proper regulation of the current space vector.
Since a voltage margin is needed during current transients following a torque request, the technique used for voltage vector saturation and current control during limitation conditions heavily affects the overall drive control stability and robustness, obviously reflecting into torque ripple and efficiency performances. In general a trade-off between dc bus voltage exploitation and current ripple exists, since operation at higher voltage amplitude (i.e. around or above U_N) causes transient voltage saturation.
In the case both speed and voltage are controlled by means of a closed-loop scheme, the steady-state operating point under flux-weakening operation can be reached by proper regulation, without the need for calculation or use of tabled characteristics from measurements. This is true even in the presence of parametric errors and non-idealities (such as those due to magnetic saturation effects), because these will only affect regulation gains by an usually acceptable amount.

Analyzed flux-weakening control schemes

Some state-of-art flux-weakening strategies are considered in this paper and their main features recalled in the next sections, i.e.:

- voltage control by means of direct (or quadrature) or phase angle of the current space vector, [1][5] (vector current control, VCC);
- voltage control by means of commanded torque and flux, [3] (torque and flux control, TFC);
- single current regulator with voltage angle control, featuring a sort of "hybrid" control behavior between flux-weakening and MTPA regions, [6][7] (SCR+VAC).

In Fig. 2 a general block diagram of a drive system incorporating speed control, current vector control, MTPA trajectory generation and flux-weakening control is shown. The output of the speed regulator could be the torque reference M_e^* or the current reference i_s^* (amplitude with sign) as a function of the adopted flux-weakening algorithm.

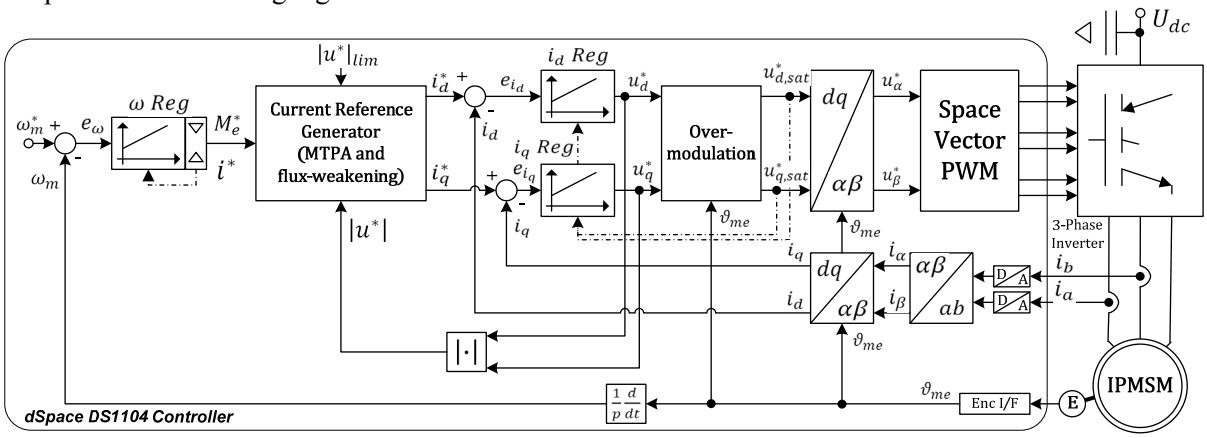

Fig. 2. Block diagram of the drive system.

In Fig. 3 the block diagrams of the considered flux-weakening strategies are shown. They share at least a general feed-back behavior, being linear in the case of direct control of motor phase voltage amplitude (VCC and TFC), i.e. Fig. 3a, b, c and d, and "switching" for the SCR+VAC approach, i.e. Fig. 3e. In the linear control of the voltage amplitude, the voltage control error is calculated by comparing the magnitude of the motor voltage reference $|u^*|$ and a certain limiting value $|u^*|_{lim} = \epsilon U_N$, where ϵ is a value smaller than one (in the linear modulation region). Slightly different is the

approach TFC where the flux-weakening is driven by the difference between the voltage reference space vector (output of current regulators) and the saturated version of that voltage vector. The voltage error is regulated to zero by commanding a variation of the dq components of the current space vector in order to operate the motor within voltage and current limitations. Main difference among the various algorithms considered in this paper is the strategy to manipulate the voltage regulation error for adjusting the value of motor currents components.

Some flux-weakening proposals consider the modulation times of the inverter states instead of the actual voltage reference. It can however be proved that this can be realized and it is equivalent to a proper over-modulation strategy of the dq components of the voltage space vector. That is the reason why in the block diagram of Fig. 2, the electrical speed ω_{me} is considered as input of the over-modulation block.

It can be noticed that at least two options can be chosen for the speed control. The schemes where the current reference space vector amplitude is considered as speed regulator output, involves non-linear relationship between current and torque, but has some implementation advantages. For example, the application of anti-windup for the speed regulator is very easy, since the limit value is constant and equal to the nominal current while, where the torque command mode is used, the limit value (which is important for anti-windup, as it will be demonstrated later) needs to be updated, decreasing above the base speed. Moreover, the choice of the dq current components from the commanded amplitude value and staying on the MTPA locus, has a low computational cost, and is usually done without the use of any tabled data. On the other hand the relationship between the commanded torque and current reference is more complex.

Synchronous current frame based voltage feedback controllers (VCC)

According to this field-weakening approach, the current vector reference coming from the MTPA calculation (fed by the speed controller), is modified by applying the output of a voltage amplitude feedback regulator, in order to achieve the desired flux-weakening effect. As shown in Fig. 3a, b, c,

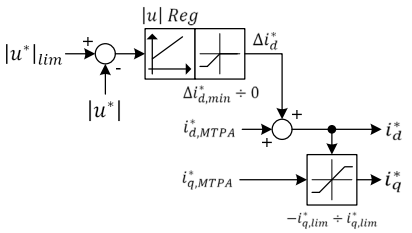

(a) variation of d current (VCC)

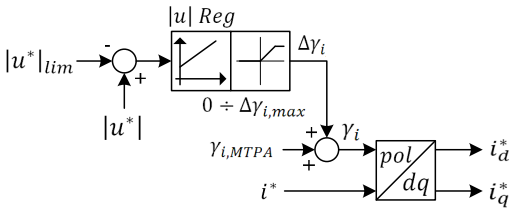

(b) variation of phase angle of current vector (VCC)

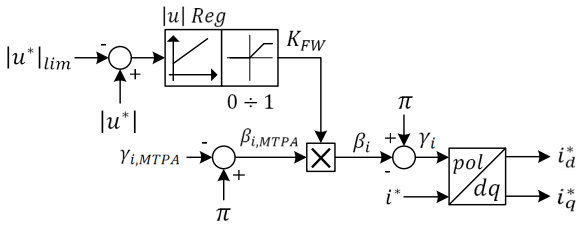

(c) proportional control of phase angle of current vector (VCC)

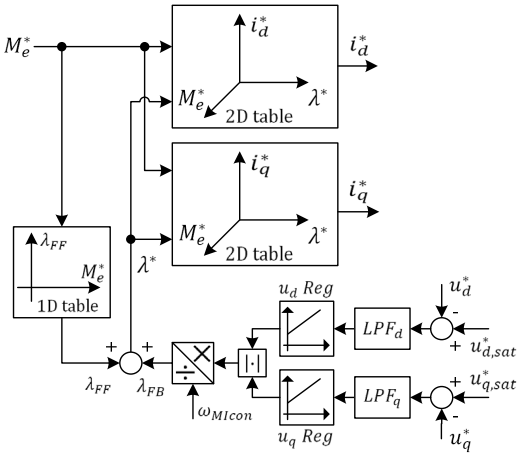

(d) feed-forward and feed-back voltage control by commanded torque and flux (TFC)

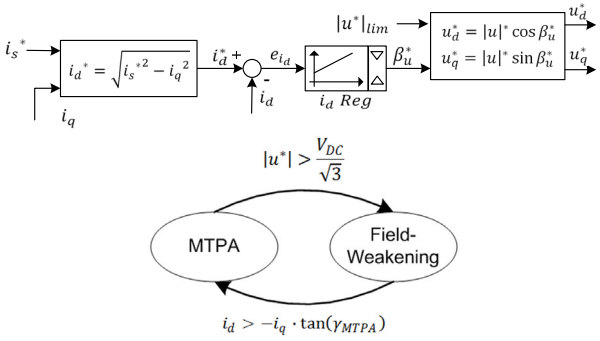

(e) single-current regulator and voltage angle control (SCR + VAC)

Fig. 3. Different strategies for flux–weakening control.

this can be done at least in three different ways, i.e. by imposing a reference for three different variables, operating on the d current component or on the current vector phase angle (and also, but it is not shown here, on the q current component).
The first algorithm is illustrated in Fig. 3a. The voltage controller R_u processes the voltage error and provides a variation Δi_d of the d component of the current space vector. That value is added to the one providing MTPA control (i.e. i_d^{MTPA}), [2][5]. The q component i_q^{MTPA} should then be processed accordingly, in order to keep the amplitude of the current space vector equal to the output of the speed regulator.
The second scheme shown in Fig. 3b directly adjusts the angle of the current space vector, whereas the amplitude $|\bar{\imath}|^*$ is provided by the speed regulator. Phase angle variation $\Delta\gamma_i$ is the output of the voltage regulator, added to the MTPA reference current vector phase.
In the scheme of Fig. 3c a proportional change of current space vector phase angle is imposed, [1], by means of the factor K_{FW}, being the output of the voltage regulator and whose value is limited in the range $[0; 1]$. The angle β_i^{MPTA} is calculated as the complementary value of the current space vector phase angle γ_i^{MTPA} with respect to π. The value of β_i^{MPTA} is then multiplied by $0 \leq K_{FW} \leq 1$. In this way, MTPA operation is maintained until voltage reaches the reference value U_{lim}, so saturation at $K_{FW} = 1$, whilst flux-weakening is obtained by reducing the value of K_{FW} towards zero, thus phase-shifting the current reference vector towards π.
Under flux-weakening operation, phase voltage amplitude is forced to the reference value by generating a current vector which is out of the MTPA trajectory, and so reaching the intersection point between the required torque hyperbola and the reference voltage ellipse. This will be the condition satisfying the voltage limit and having the lower current vector magnitude. A higher d-axis current component or a phase angle lying on the left of the MTPA trajectory results in weakening the flux value, and so reducing steady-state voltage amplitude. Proper limitation of the voltage regulator output ensures the current reference phase is always limited between the MTPA angle for the commanded current amplitude and the negative d-axis (i.e. always to the left with respect to the MTPA trajectory), so that MTPA is followed until flux-weakening is strictly needed.
From a dynamical point of view, each of these three schemes has different gain characteristics, but they all share the same underlying approach and act on a portion of the system which has the same small-signal behavior, i.e. specifically the transfer function relating the current vector to the voltage amplitude. They can thus be studied together, just applying light modifications to the gain analysis (see next sections and [9]).

Feed-forward and feed-back voltage control by commanded torque and flux (FTC)

A mixed feed-forward and feed-back strategy based on torque and flux control is considered in Fig. 3d, [3]. The dq current components are a function of both commanded torque M_e^* and proper flux level λ^* and are obtained by means of two two-dimensional look-up tables. Both analytical (i.e. from motor model) and measured values can be considered to build up the tables. The flux magnitude command is obtained as the sum of two contributions, namely λ_{FF} and λ_{FB}. The first one is obtained in a feed-forward manner as a function of commanded torque through an additional look-up-table, depending on motor speed. While MTPA control substantially relies on the feed-forward path, the voltage limitation feed-back modifies the flux reference. An error signal is calculated as the difference between the magnitude of the synchronous current regulators outputs and the saturated voltage (where the saturation is imposed by PWM modulator over the six-step hexagon or an inner hexagon). This path only contains low-pass filters (there are no pure integrators), then does not provide steady-state null error (i.e. no voltage saturation at all), but allows to use an average voltage range comprised in between the inscribed circle and the outer circle with respect to the physical limit being the hexagon (whose radiuses are respectively $1/\sqrt{3}$ and $2/3$ of the dc bus voltage). The relationship between the gain on this path ($1/\omega_{MIcon}$) and the resulting average voltage limit value is quite complex, and has not been provided in the reference paper. However, it can be stated that a higher gain leads to a lower non-linear modulation, while a lower gain moves the PWM modulation range towards the six-step mode.

Single current regulator and voltage angle control (SCR+VAC)

A very recent and completely different approach is the one shown in Fig. 3(e), [6][7]. Standard MTPA vector current control is performed below base speed (having the speed regulator output as the current magnitude reference), whilst the phase angle of the voltage space vector (instead of current) is imposed in flux-weakening region to achieve d-axis current control. During this last mode, the speed control loop provides a reference value for d current regulator, whose output represents the phase angle of voltage space vector. The amplitude is fixed at a constant value $|u|^*$ being less than or equal to the voltage capability of the inverter, given the applied modulation strategy. The reference d axis current i_d^* is calculated from the speed regulator output i_s^* and the measured quadrature current i_q, so that their quadratic sum must satisfy the current limit at steady-state. Since a direct current control is not performed on both axes, it does not prevent modulus of current from being out of the specified limit for sensible time amounts. The condition for passing from MTPA to single current regulation is the voltage amplitude (i.e. the current regulators output modulus) being higher than the voltage limit $|u^*|_{lim}$, while the opposite transition happens when the current vector angle is lower than the MTPA reference phase.

A raw comparison among the considered flux-weakening approaches

The considered flux-weakening techniques can be evaluated according to various aspects, including effectiveness in exploiting the available dc bus voltage, implementation complexity/requirements and dynamical properties.

The main advantages of the synchronous current frame based controllers (VCC) are related to their simple implementation, providing a seamless integration with the standard vector control, also leading to an automatic management of transitions between MTPA and flux-weakening control. This means that any traditional MTPA technique can be used, besides the recently introduced on-line tracking, [10][11]. In fact, the flux-weakening controller produces no effect until the voltage limit is exceeded and, thanks to a proper anti-windup action on the PI regulator, it guarantees smooth operation when working across the limitation boundary (between MTPA and flux-weakening regions). Moreover, it does not require any look-up-table, thereby no discretization effect is introduced, and large memory, processing performance and parameter-dependent off-line calculations are not needed. A gain scheduling could also be implemented to adapt the regulator's dynamics to the varying operating conditions (see next sections for details), either analytically or by using look-up-tables. But, in this last case, discretization is present in the stored gain values only, which typically requires a lower number of points and generates lower noise on the controlled variables with respect to the case of feed-forward approaches. Finally, all the controller gains and limitations are obtained from few motor and inverter parameter values, such as the voltage-current limits, maximum speed, inductances and permanent magnet flux linkage amplitude.

The FTC technique involves a large memory usage in order to store the look-up-tables, and a complex implementation to manage some out-of-domain operating conditions. Moreover, an extensive off-line measurement and post-processing effort should be carried out to fill in the tables, making it not feasible to apply any on-line tuning based on just the main motor and inverter parameters. An advantage in the overall control could be pointed out in the case of strong magnetic saturation effects, but this will likely be more evident under MTPA conditions, while has little influence on the flux-weakening operation, since this last operating region relies mainly on the feed-back component of the voltage controller.

In the referenced paper, the advantage of this approach is claimed to be related to the lack of an anti-windup back-calculation for the current regulators. In fact, it is shown that the interaction between current regulators anti-windup algorithms (which limiting values are taken from the over-modulation calculation) and the voltage feedback path are conflicting each other during quasi-six step operation. The simulations carried out for the scheme in Fig. 3b however show that the adopted feedback controller more or less avoids saturation of the current regulators, if current control is attained in flux-weakening conditions. Therefore anti-windup is never active. Therefore the over-modulation mode can be adopted too, but a torque ripple arises due to voltage limitations on the limit hexagon, similarly to the approach of Fig. 3d.

The SCR+VAC approach demonstrates weak stability and high sensitivity to gain parameters. In particular, it would be difficult to ensure the current magnitude value will obey the nominal limit during

transients, since only the d axis component is being directly controlled. For the same reason, it is also difficult to find a relationship between the instantaneous values of the controlled variables and the resulting torque. On the other hand this method ensures the maximum exploitation of the available voltage ($U_{dc}/\sqrt{3}$) during field-weakening operation.
Smooth transition between the two different control regions is claimed in the reference paper, but the experimental results show some oscillations, especially if looking at the currents in the synchronous reference frame. This result can be expected, since the method relies on steady-state equations and current vector components are not both directly controlled. This is the main disadvantage with respect to other techniques, as it means that torque generation and current limitation is not always under full control.

Flux-weakening controller design: a novel design approach

Referring to the scheme in Fig. 3b, a novel theoretical analysis of the voltage control loop adopted in the flux-weakening operating region has been carried out, showing that optimized design of the controller can be obtained for each speed condition. Therefore stability properties can be fixed and maximization of the bandwidth of the loop can be obtained by a proper choice of the voltage control loop transfer function, leading to the increment of the available dc bus voltage exploitation.
The voltage control loop adopted in the flux-weakening operating region can be represented by means of a non-linear block diagram, as shown in Fig. 4. A first order approximation of control delays taking into account the discrete time implementation and pulse-width-modulation have been considered both in the forward loop and in the feedback loop. Electrical angular speed Ω_{me} is considered at steady-state condition, as the dynamical behavior of the electrical quantities is analyzed. Voltage regulator $R_u(s)$, current regulators $R_{i_d}(s)$ and $R_{i_q}(s)$, control delays $CD(s)$ and motor model $\boldsymbol{M}_{\Omega_{me}}(s)$ (matrix) transfer functions are shown in the diagram. Λ_{mg} is the permanent magnet flux-linkage, R_s, L_d and L_q are phase resistance and synchronous inductances respectively. The equivalent analytical model is highly non-linear due to the presence of angular speed dependent terms (i.e. back-electromotive force) as well as non-linear terms (both transcendent and modulus functions).
Linearization of the voltage control loop of Fig. 4, which is valid in the neighborhood of a certain operating condition, allows to study the dynamical behavior in the Laplace domain by means of the open-loop transfer function. A comprehensive transfer function linking reference current vector angle γ^* to voltage amplitude $|u^*|$, can be obtained (details can be found in [9]), i.e.:

$$\frac{|u^*|(s)}{\gamma^*(s)} = \begin{bmatrix} \frac{\bar{U}_d}{U_{lim}} & 0 \\ 0 & \frac{\bar{U}_q}{U_{lim}} \end{bmatrix} \boldsymbol{R}_{i_{dq}}(s)[\mathbf{I}_{2\times 2} - \boldsymbol{CC}(s)] \begin{bmatrix} -\bar{I}_s \sin\bar{\Gamma} \\ \bar{I}_s \cos\bar{\Gamma} \end{bmatrix} \tag{5}$$

where $\boldsymbol{R}_{i_{dq}}(s)$ is a diagonal matrix of current regulators, $\boldsymbol{CC}(s)$ is the closed-loop current control transfer function and $\mathbf{I}_{2\times 2}$ is the 2^{nd} order identity matrix. Upper-case over-lined symbols represent the operating point values.

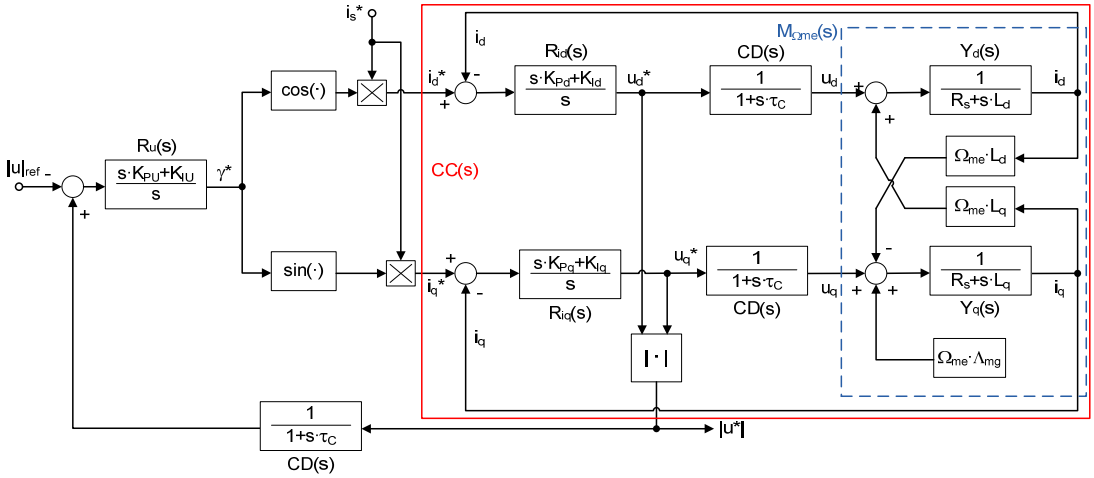

Fig. 4. Voltage vector amplitude control loop model.

Referring to the block diagram of Fig. 4, a set of open-loop transfer functions parameterized by angular speed value can be calculated by including the voltage regulator $R_u(s)$ and the control delay model of the feed-back loop, as shown in Fig. 5 (left). Control bandwidth, stability range and margins can easily be calculated for each operating condition. Analysis of those curves shows that heavy variation of static gain occurs (about $20dB$ in this case).

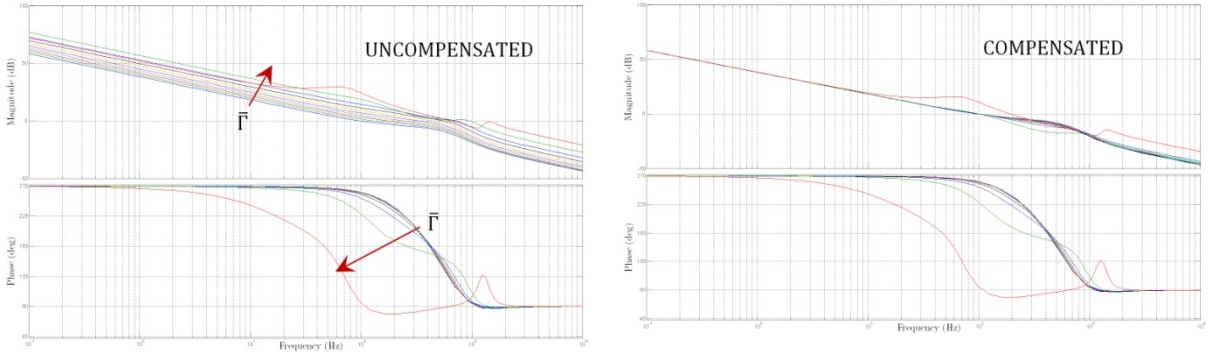

Fig. 5. Open-loop responses at various speeds (i.e. current angle $\bar{\Gamma}$), $\bar{\Gamma} \in [\Gamma_{\mathrm{MTPA}}\,;\pi - 0.01]$, $\overline{I_s} = I_{sN}$.

A simple approach to guarantee a proper stability margin for each operating condition is to dynamically vary the static gain of the voltage controller, i.e. adaptation of the controller by gain scheduling, compensating for the plant static gain variations. Accurate design of the closed-loop response bandwidth is therefore possible, approximately maintained for the whole needed speed range, as shown in Fig. 5 (right).

From a dynamical point of view, each of these three schemes has different gain characteristics, but they all share the same underlying approach and act on a portion of the system which has the same small-signal behavior, i.e. specifically the transfer function relating the current vector to the voltage amplitude. They can thus be studied together, just applying light modifications to the gain analysis. Same dynamical analysis can be repeated in the case of flux-weakening schemes of Fig. 3a and Fig. 3c. Also a fourth flux-weakening controller where q-axis current is the voltage regulator output can be considered. It can be demonstrated that the sensitivity functions (i.e. the static gain of the open-loop transfer functions) are different among the various control choices, i.e. heavy gain variation occurs in the deep flux-weakening region, [9]. This is especially true when using a scheme in which d-axis current is the voltage regulator output and was expected since circular current trajectory (constant amplitude) has a high slope, for angle values near to π. The minimum variation of the static gain occurs adopting the current space vector angle γ as the control output. Even in that case, however, the voltage control loop static gain exhibit large variations over the whole speed operating range, thus suggesting an adaptive voltage controller in order to provide a globally optimized bandwidth.

The flux-weakening control of Fig. 3c provides therefore a similar dynamical behaviour to that of Fig. 3b, but allowing a little advantage from the implementation point-of-view as the PI regulator output (and the related anti-windup back calculation) is always within the range $[0\,,1]$.

Simulation results

Comparative simulations between the discussed flux-weakening control schemes have been carried out under the Matlab/Simulink environment. A motor drive system for home appliances has been considered, whose main parameters are listed in Table I (reported after the conclusions). A test speed reference pattern is considered following a rising and a falling ramp, each followed by speed and torque steady-state conditions. The ramp slope is set to the maximum acceleration achievable by the drive, given the torque limit under MTPA control and the load inertia. This means that, when entering the flux-weakening region, the actual speed slope decreases with speed. The reduced value of produced torque depends on the voltage limitation imposed by the considered flux-weakening controller, and then qualifies the voltage exploitation characteristics of the adopted technique or, from another point-of-view, allows to evaluate the maximum torque as a function of speed. The results show a similar steady-state behavior, as expected from the qualitative analysis. Some differences arise during transient conditions.

The scheme providing the best stability is the vector control based one with the proposed adaptation of the voltage regulation loop gains (results are shown in Fig. 6), since it maintains full current control under all of the operating conditions, even when a voltage limitation outside the linear region (quasi-six step operation) is considered, i.e. the voltage margin is chosen to be $\epsilon = 1.05$. The experienced heavy ripple on voltage, currents and torque can therefore be justified by the over-modulation condition. Another interesting feature is that the method does not require any switching among different controllers and is only based on feedback regulation. This last characteristic reduces discontinuities and ensures null steady-state voltage error, due to the integral action in the feedback branch.

Fig. 7 shows the results of the FTC flux-weakening approach in the same quasi-six step operating conditions. One can notice that the speed transient duration is exactly the same of the VCC approach, thus proving that FTC adds a redundant complexity to the flux-weakening control scheme. Really FTC experiences some problems during transient conditions due to the low-pass action of the feedback loop, that also does not incorporate any integration feature, leading to non-zero steady-state voltage control error.

In Fig. 8 SCR+VAC flux-weakening is considered. Good steady-state results in particular for the voltage are obtained, but current limitations cannot be obeyed. A short but heavy overshoot is present at the torque demand transitions, which may be or not acceptable, depending on the application, but does not provide a corresponding torque boost, demonstrating a transient inefficiency.

It must be pointed out that a dynamical analysis is available only for the VCC based technique, where the gains have been adjusted based upon the open-loop transfer function bode plots, as discussed in the previous section. Since in the other two flux-weakening schemes gains have been tuned empirically, it can be possible that the best performances are not fully obtained.

Finally, in order to demonstrate the benefit of the proposed gain scheduling approach for the VCC flux-weakening scheme, a comparison between fixed and gain scheduling voltage controllers (designed for the same maximum speed value of 22000 $[rpm]$) is shown in Fig. 9. A load torque step disturbance (low-pass filtered at 1 kHz) at steady-state and high-speed condition is applied and the

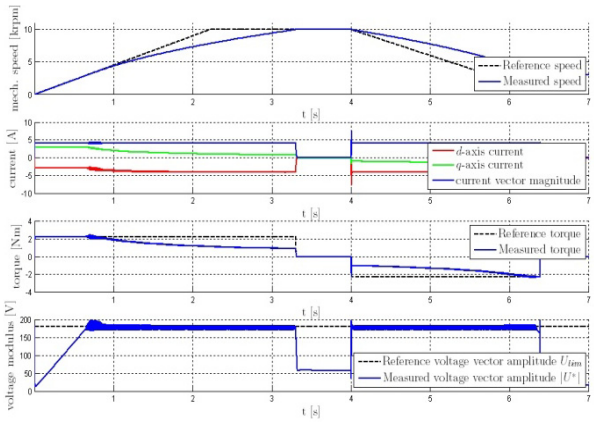

Fig. 6. Speed response of VCC.

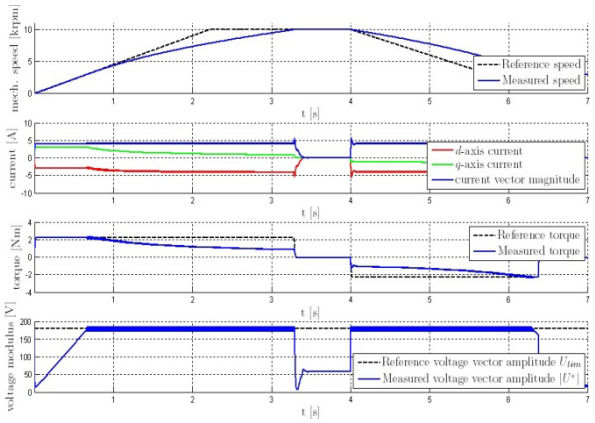

Fig. 7. Speed response of FTC.

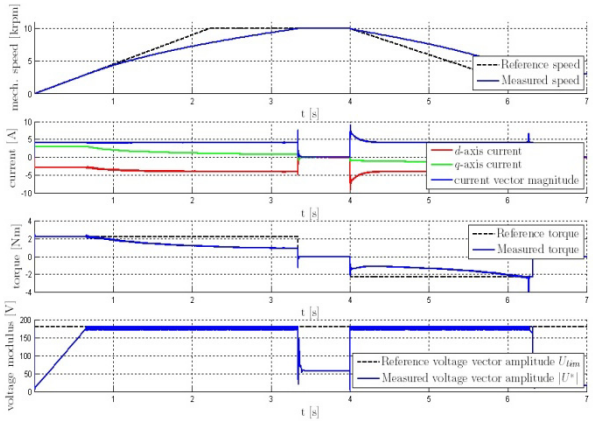

Fig. 8. Speed response of SCR+VAC.

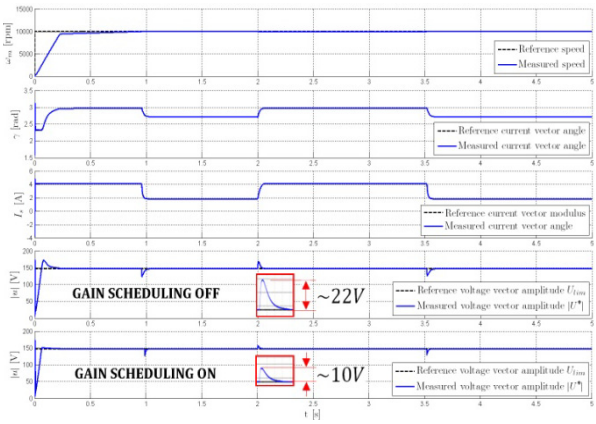

Fig. 9. Torque disturbance rejection (10000 rpm, VCC without/with gain scheduling).

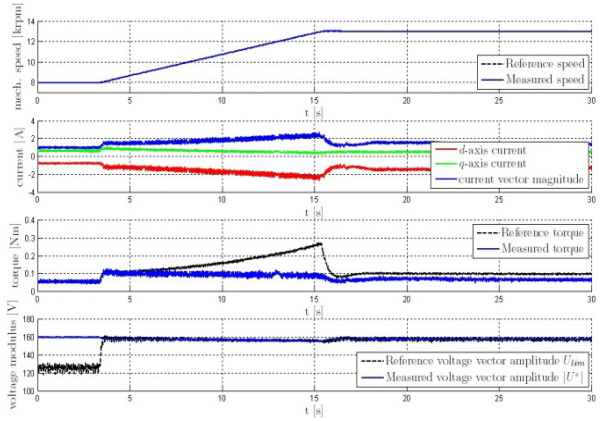

Fig. 10. Speed reference from 8000 to 13000 rpm (VCC, angle multiplicative factor flux-weakening control, experimental).

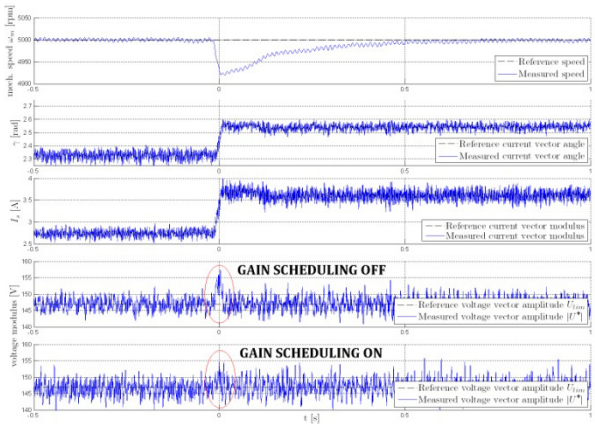

Fig. 11. Load torque disturbance rejection (5000 rpm, VCC without/with gain scheduling, experimental).

response of the voltage control loop analyzed. The reference voltage has been chosen to be lower than the maximum allowable voltage of the inverter in order to study the behavior of the controller in non saturated conditions. As shown in the zoomed boxes the peak voltage reached during load torque removal is much lower when gain scheduling controller is considered, thus confirming the reliability of the proposed analysis and the effectiveness of the gain adaptation. *Optimization of voltage control loop allows therefore to increase voltage limiting value thus maximizing bus voltage exploitation*.

Experimental results

The three VCC flux-weakening approaches discussed above have been verified by means of an experimental test bench equipped with an IPM motor for home appliances and a controlled induction motor acting as a load. Differently from the simulated model, in this case the voltage amplitude reference is calculated on-line as a function of the actual value of the dc bus voltage, ensuring that the PWM modulation always remains inside the linear range, with an utilization factor $\epsilon = 0.95$. Since some measurement noise and inverter non-idealities is present in the experimental system, proper filtering is applied to the measured dc bus voltage, considering that the dynamical performances of the voltage control is lower than those of the current control.

The results of the tests with the three flux-weakening approaches are very similar, even if some minor differences arise, mainly due to the different values of the voltage controller gains. The results of the flux-weakening adopting a regulation through a multiplicative factor on the current phase angle are shown in Fig. 10. One can notice that a proper voltage and current control is obtained both in transient and during steady-state conditions. The reference voltage amplitude is slightly higher at the end of the speed transient as the dc bus voltage increases due to a reduction of the sunk power. The reference torque is the value of the torque that the MTPA would provide in that condition and the "measured" torque is indeed an estimated value based on the motor parameters, as no torque sensor is available in the experimental setup.

In the result of Fig. 11 a similar test to Fig. 9 is considered, showing that a good agreement is obtained between theoretical analysis and experiments. It should be noted that the experimental set-up does not allow a step torque disturbance generation as in the simulation results, since an induction motor drive is adopted as load in this case. The design and optimization of the voltage regulator's gains are done by considering the open-loop transfer function (magnitude and phase) of the voltage regulation loop at, e.g., 10000 rpm. When a lower value of the speed is commanded, i.e. 5000 rpm, and voltage regulator's gain is kept constant, a relatively high value of actual voltage overshoot is obtained as response to a sudden variation of load torque. As a higher gain margin is available at lower speed, voltage regulator's gain can be increased consequently and response of voltage regulation loop to the same load torque variation provides a lower dynamical error. In the results noise coming from the voltage measurement system has to be taken into account for a correct comparison. Another test in the same operating conditions, with gain scheduling activated and with a higher value of regulator's gain (increase of 50% is considered, i.e. 3 dB) provides instability, thus proving the reliability of the theoretical analysis.

Conclusions

Implementation issues and performances of some state-of-art flux-weakening algorithms have been analyzed. Due to the relatively simpler structure, the methods based on the voltage control by means of direct (or quadrature) or phase angle of the current space vector, differently from those based on flux-torque reference or direct voltage vector control, can be easily implemented inside the standard vector controlled drives, allowing to easily obtain stability, robustness and good performance. The novel theoretical analysis of the voltage control loop dynamics provides a useful means for the optimization of the dynamical performance of the flux-weakening controller in the whole speed range.

Table I: Motor, inverter and control parameters

Pole pairs, pp	2
Stator resistance, R_s	2.86 [Ω]
Direct inductance, L_d	0.0119 $[H]$
Quadrature inductance, L_q	0.0869 $[H]$
PM flux linkage (amplitude), Λ_{mg}	0.028 $[Vs]$
Rated current, $\|i\|_{n,rms}$	3 $[Arms]$
Electromagnetic torque, $T_{e,}@500rpm$	1.3 $[Nm]$
Electromagnetic torque, $T_{e,}@18000rpm$	0.4 $[Nm]$
dc bus voltage, U_{DC}	300 $[V]$
Switching and control frequency, f_{SW}, f_C	10 $[kHz]$

References

[1] J. Wai and T. M. Jahns, "A new control technique for achieving wide constant power speed operation with an interior PM alternator machine", in *Conference Records of the 36th IEEE Industry Applications Society Annual Meeting*, volume 2, pages 807–814, Chicago, IL, Sept. 30–Oct. 4, 2001.

[2] J.-M. Kim, S.-K. Sul, "Speed control of interior permanent magnet synchronous motor drive for the flux weakening operation," *IEEE Trans. on Industry Applications*, vol. 33, no. 1, pp. 43 –48, 1997.

[3] T.-S. Kwon, G.-Y. Choi, M.-S. Kwak, S.-K. Sul, "Novel Flux-weakening Control of an IPMSM for Quasi-six-step Operation," *IEEE Trans. on Industry Applications*, vol. 44, no. 6, pages 1722–1731, Nov./Dec., 2008.

[4] Y.-D. Yoon, W.-J. Lee, S.-K. Sul., "New flux weakening control for high saliency interior permanent magnet synchronous machine without any tables," in *Proc. of the European Conference on Power Electronics and Applications*, pages 1–7, Aalborg, September 2–5, 2007.

[5] N. Bianchi, B. N. Bolognani, M. Zigliotto "High performance PM synchronous motor drive for an electrical scooter," in *Conference Records of the 35th IEEE Industry Applications Society Annual Meeting*, vol. 3, pp. 1901–1908, Rome, Oct. 8–12, 2000.

[6] L. Zhu, S. Xue, X. Wen, Y. Li, L. Kong, "A new deep field-weakening strategy of IPM machines based on single current regulator and voltage angle control," in *Proceedings of the Energy Conversion Congress and Exposition*, pp. 1144 – 1149, Atlanta, GA (USA), 2010.

[7] Y. Zhang, L. Xu, M.K. Guven, S. Chi, "Experimental Verification of Deep Field Weakening Operation of a 50 kW IPM Machine by Using Single Current Regulator," *IEEE Trans. on Industry Applications*, vol. 47, no. 1, pp. 128-133, 2011.

[8] S. Chi, L. Xu, "A special flux-weakening control scheme of PMSM - incorporating and adaptive to wide-range speed regulation," in Proceedings of the CES/IEEE 5th International Power Electronics and Motion Control Conference, vol. 2, pp. 1 –6, 2006.

[9] S. Bolognani, S. Calligaro, R. Petrella, "Optimal Voltage Feed-Back Flux-Weakening Control of IPMSM," submitted for presentation at the 37th Annual Conference of the IEEE Industrial Electronics Society, 2011.

[10] S. Bolognani, R. Petrella. A. Prearo, L. Sgarbossa, "Automatic Tracking of MTPA Trajectory in IPM Motor Drives Based on AC Current Injection," *IEEE Trans. on Industry Applications*, vol. 47, no. 1, pp. 105-114, Jan.-Feb. 2011.

[11] S. Bolognani, R. Petrella, A. Prearo, L. Sgarbossa, "On-Line Tracking of the MTPA Trajectory in IPM Motors Via Active Power Measurement," *Proc. of the XIX International Conference on Electrical Machines*, 6 8 September, Rome, Italy, 2010.